REVIEW ARTICLE

MICROSCALE THERMAL BUBBLE FORMATION: THERMOPHYSICAL PHENOMENA AND APPLICATIONS

Liwei Lin

Department of Mechanical Engineering and Applied Mechanics, University of Michigan, Ann Arbor, Michigan, USA

This work addresses the thermophysical phenomena of bubble formation by using solid-state microheaters and recommends specific directions for future applications. Microscale bubble formation has become an important actuation mechanism for microfluidic machines in the emerging field of microelectromechanical systems (MEMS). Characterization of microbubble formation mechanisms leads to new scientific research in microscale heat transfer and provides design guidelines for bubble-powered micromachines. A review of theoretical bases describing heat transfer processes of solid-state microheaters is followed by a discussion of the thermophysical phenomena of microbubble nucleation mechanisms. Engineering challenges are illustrated with existing and potential applications including ink-jet printers, microbubble-powered mechanical actuators, microbubble valves, and microbubble pumps.

Modern microfabrication technologies in microelectromechanical systems (MEMS) are shrinking mechanical devices into micro- and nanometer scales [1]. The trend of miniaturization has brought unprecedent research interest in microscale heat transfer [2–4] and inspired innovative devices based on microscale thermophysical phenomena. For example, thermal bubble-powered ink-jet printers have combined microscale heat transfer and MEMS technologies for practical application [5, 6]. Many other heat transfer phenomena in the microscale are expected to provide more new and practical directions in the area of MEMS.

Microheater is one of the key elements in microscale heat transfer, and this article discusses microscale bubble formation by using polysilicon microheaters. Figure 1*a* shows a schematic diagram of a polysilicon microheater that has been used to generate individual, controllable thermal microbubbles in working liquids [7]. Being a standard integrated circuit (IC) "gate" material [8] in metal oxide silicon field-effect transistors (MOSFETs), polysilicon microheaters can be easily integrated with microelectronics to enhance control and signal-processing capabili-

NOMENCLATURE

c	specific heat, $\mathrm{W/m\,^\circ C}$	α	thermal diffusivity, $\mathrm{m^2/s\,^\circ C}$
F	excess heat conduction shape factor	ε	variable in the heat equation, $\mathrm{^\circ C/m^2}$
h	thickness, m	ρ	density, $\mathrm{kg/m^3}$
J	current density, $\mathrm{A/m^2}$	ξ	coefficient of resistivity change with
k	thermal conductivity, $\mathrm{W/m\,^\circ C}$		temperature, $\mathrm{^\circ C^{-1}}$
L	length of the microheater, m		
r_c	radius of critical cavity in Hsu's analysis, m	**Subscripts**	
R	resistivity, Ω m		
t	time, s	o	silicon dioxide
T	temperature, $\mathrm{^\circ C}$	p	polysilicon
T_{ref}	reference temperature in the heat	sat	saturation
	equation, $\mathrm{^\circ C}$	ss	steady state
x	coordinate, m	∞	ambient

ties of microdevices. Several MEMS devices have been built with polysilicon microheaters. Figure 1*b* is a sketch of a bubble-powered microactuator that utilizes the actuation force of microbubbles generated by polysilicon microheaters to push micromechanical structures [9]. Other research directions and engineering challenges in the area of microbubble formation have been proposed, including microbubble pumps in microneedles [10] and micro steam engines [11].

This article addresses microscale bubble formation by using solid-state polysilicon microheaters and recommends specific directions for future applica-
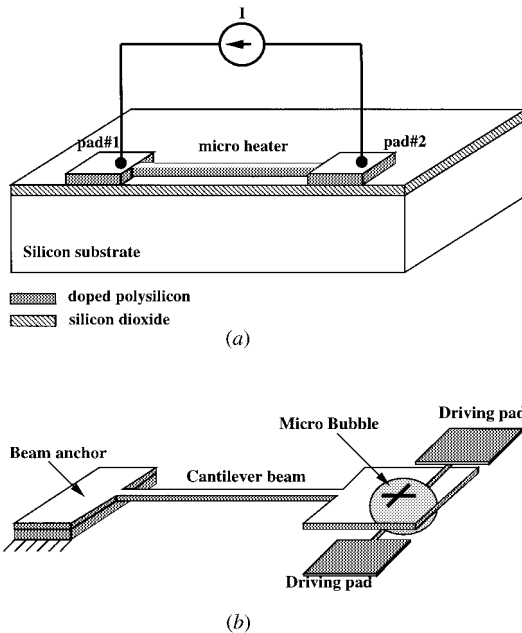
(*a*)

(*b*)

Figure 1. Schematic illustrations of (*a*) a solid-state polysilicon resistive heater and (*b*) a microbubble powered actuator [13].

tions. The general fabrication process of MEMS microstructures is first presented. This is followed by a review of theoretical bases describing the heat transfer processes of solid-state microheaters. A discussion of bubble nucleation mechanisms based on microheaters is continued in a separate section. Preliminary results in the application areas of microbubble-powered mechanical actuators, microbubble valves, and microbubble pumps are discussed at the end.

MICROSCALE DEVICE FABRICATION

The fabrication process of MEMS microstructures follows general IC manufacturing technologies. There are three basic IC processes: thin-film deposition, lithography, and etching [12]. Thin-film deposition is used to grow thin layers of microelectronics materials such as silicon oxide, silicon nitride, gold, aluminum, and others. In a manufacturing facility, both the thickness and uniformity of thin-film deposition processes can be well controlled. The lithography process consists of three steps: photoresist coating, exposure, and development. A thin layer of photoresist is spin-coated on the surface of the thin-film-deposited substrate. A photolithography mask is then used to define the desired patterns on the photoresist through exposure and development processes. The patterned photoresist serves as the mask during the etching process and is removed after completion of the etching process. Unwanted parts are etched away by either wet chemical etching or dry plasma etching processes. New runs of processes including thin-film deposition, lithography, and etching may continue to complete the fabrication of microstructures. For standard IC devices such as MOSFETs, it may take 10 to 20 masks. Some MEMS devices are simple and take very few masks, such as the fabrication of solid-state polysilicon microheaters to be described below [7].

The overall process sequence is illustrated in Figure 2. Fabrication begins with clean prime wafers. Thermal oxidation is first used to create a thin layer of silicon dioxide, which serves as both the electrical and thermal insulating material. Wafers are then transferred into a low-pressure chemical vapor deposition (LPCVD) polysilicon furnace for deposition of in-situ phosphorus-doped polysilicon. Annealing in nitrogen environment is then followed to activate the dopants in the polysilicon layer. The shape of microheaters is defined by the lithography
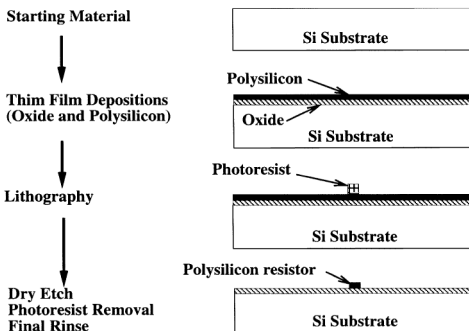

Figure 2. The fabrication process for polysilicon microheaters.
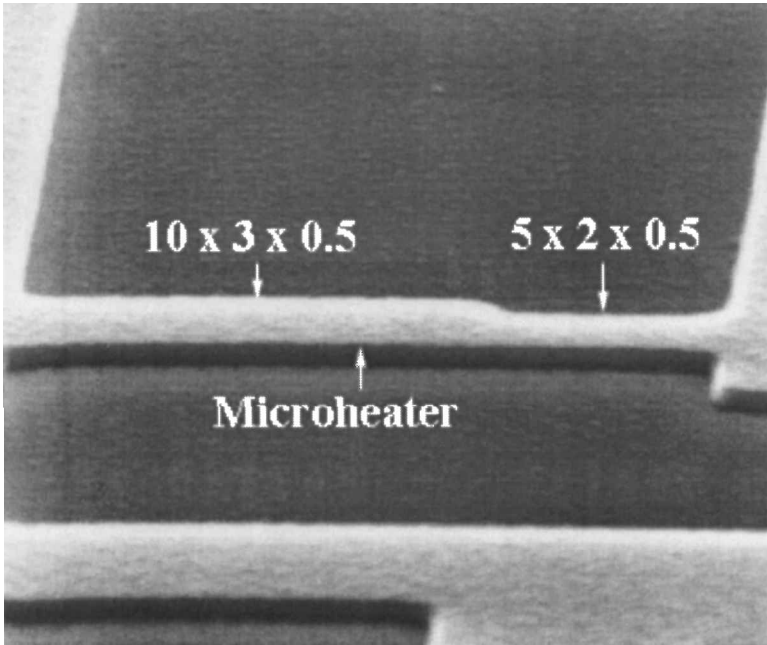
10 x 3 x 0.5 5 x 2 x 0.5

Microheater

Figure 3. A SEM micrograph of a fabricated microheater.

process, and unwanted polysilicon is etched away during the dry plasma etching process. After the photoresist is removed, the process is completed with a final rinse in deionized (DI) water. Figure 3 is a scanning electron microscope (SEM) micrograph showing a fabricated microheater. This microheater has two different lineshape portions, (10×3) and (5×2) μm^2, respectively, with thickness of about 0.5 μm. When a current is applied, the thinner portion is expected to have a higher current density and a higher temperature profile. More complicated microdevices require additional processes and masks [11, 13, 14].

MICROSCALE HEAT TRANSFER PROCESS

Microscale heat transfer processes of microheaters presented here follow conventional heat transfer models developed for macro structures. Heat generation by the electrical current, heat conduction, convection, and radiation are calculated separately and then combined based on the conservation of energy. It is found that heat conduction to the silicon substrate dominates the overall heat transfer process. Both heat convection and heat radiation have little effect in the environment, as illustrated in Figure 1a. The effectiveness of heat convection is examined by Rayleigh's number [15]. It is found that Rayleigh's number is about 0.01 for the described geometry and is much less than the critical magnitude for free heat convection to occur [16]. The heat radiation term is much smaller than the heat conduction term for operation in low temperature ranges to generate thermal bubbles.

Based on both the heat generation and heat conduction processes, a one-dimensional electrothermal model is established and has been described previously [7]. The second-order partial differential heat equation is derived as

$$\frac{\partial^2 T}{\partial x^2} = \frac{1}{\alpha_p} \frac{\partial T}{\partial t} + \varepsilon(T - T_{\text{ref}}) \tag{1}$$

where T is the temperature along the solid-state polysilicon microheater, t is time, and α_p is the thermal diffusivity of polysilicon. Both ε and T_{ref} are parameters that are functions of heater dimensions and thermal properties. These symbols are summarized below:

$$\alpha_p = \frac{k_p}{c_p \rho_p} \tag{2}$$

$$\varepsilon = \frac{k_o F}{k_p z h_o} - \frac{J^2 R_p \xi_p}{k_p} \tag{3}$$

$$T_{\text{ref}} = T_\infty + \frac{J^2 R_p}{k_p \varepsilon} \tag{4}$$

A shape factor, F, is used to account for the excess heat conduction to the environment [17]. Since shape factor depends on the geometry and properties of both solid-state heaters and the environment, numerical simulations are required to calculate their values [16].

Equation (1) is solved subject to the initial and boundary conditions. It is assumed that both ends of microheaters remain at ambient temperature during the heating process and microheaters are initially at ambient temperature before heating.

$$T(x = 0, t) = T_\infty \tag{5}$$

$$T(x = L, t) = T_\infty \tag{6}$$

$$T(x, t = 0) = T_\infty \tag{7}$$

For microheaters with uniform width as illustrated in Figure 1a, steady-state temperature solutions along the solid-state microheater are derived as

$$T(x)_{\text{ss}} = T_r - (T_r - T_\infty) \frac{\cosh[\sqrt{\varepsilon}(x - L/2)]}{\cosh(\sqrt{\varepsilon} L/2)} \tag{8}$$

The maximum temperature occurs at the center of a microheater. For micro-heaters with irregular shapes as illustrated in Figure 3, the temperature profile is simulated by finite-element analysis. Simulation results shows that the highest temperature occurs at the narrower portion, about 11.6 μm away from contact pad

at the left. Moreover, a temperature of 300°C can be reached under an input current of 11 mA [7].

Transient solution can be solved analytically or numerically by specifying both boundary and initial conditions for Eq. (1). It has been found that the transient decay time of microheaters is very short. For microheaters with the geometry of $50 \times 2 \times 0.5 \ \mu m^3$, it takes about 10 μs to bring the temperature to 300°C for an input current of 11 mA. On the other hand, temperature will drop to less than 50°C in 2 μs after removing the 11-mA input current on this microheater [16]. A detailed 3-D heat conduction analysis based on a molecular cluster model has been derived based on the derivations described in this section [18, 19].

MICROSCALE THERMOPHYSICAL PHENOMENA

Investigations on boiling experiments using "small" size heaters have been reported since decades ago. Small metal wires with diameters from 0.0005 to 0.081 in. have been used in pool or subcooled boiling studies [20−22]. Heated small patches have also been used in force boiling or turbulent flow tests [23−25]. Distinct differences in boiling experiments by solid-state polysilicon microheaters are identified. The most significant one is that a single, controllable microbubble instead of scattered bubbles is generated by microheaters. Moreover, bubble nucleation mechanisms face new challenges, since these microheaters have extremely small sizes. Large cavities that exist on macromachined surfaces are not likely to appear on these microheaters. Established cavity theories [26−28] for bubble nucleation in pool boiling may no longer be applicable for microheaters. In this section, both experimental and theoretical investigations on bubble nucleation mechanisms by solid-state microheaters are discussed.

Experimental Observations

Fabricated microheaters are first immersed in working liquids such as Fluorinert [29] or DI water for testing. All tests are performed under a probe station, at room temperature, 1 atm, and reported previously [7]. Bubble formation processes are observed via a microscope, photographed by Polaroid films, and recorded on video tape. In contrast to pool boiling phenomena, steady-state microbubbles can be maintained in microscale tests. This interesting phenomenon may be achieved when the evaporation rate of working liquid is equal to the condensation rate of hot vapor bubbles. Figure 4 shows that a steady-state microbubble is generated in FC43 liquid, which has a diameter of about 2 μm. The geometry of this microheater is shown in the SEM microphoto of Figure 3. This experiment is conducted by first supplying a high input current of about 12 mA, which gives a temperature of about 300°C. A thermal microbubble is nucleated (the critical temperature of FC43 is 294°C). After nucleation, the input current is reduced to about 9.5 mA and a small microbubble with a diameter of about 2 μm is maintained as shown in Figure 4. Decreasing the input power will kill the microbubble. The observation that a high input power is required to generate microbubbles while microbubbles disappears at a lower input power is similar to but not exactly the same as the bubble hysteresis phenomenon described by Bakhru and Lienhard [22]. It is also
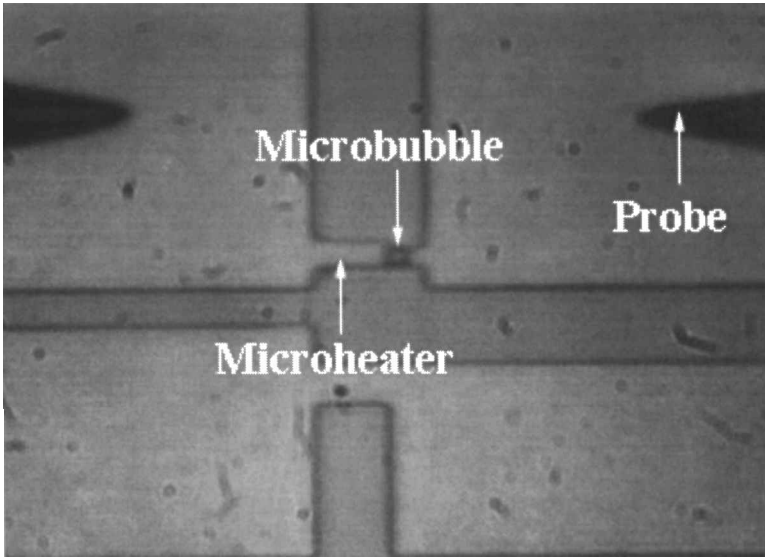
Figure 4. A single, stable bubble 2 μm in diameter is generated.

noted that the microbubble is stuck to the hottest point of the microheater due to the strong Marangoni effect around the microheater. Increasing the input power, on the other hand, will increase the size of the microbubble. Within a certain range, the size of the microbubble is controllable by adjusting the input power. The bubble will experience uncontrollable growth if its size has passed an upper limit, which may depend on the geometry and properties of both microheaters and the working liquid. A big microbubble of about 500 μm in diameter can be seen in Figure 5. The microbubble then detaches the substrate and collapses. The objective lens has been changed in this photo so that the surrounding microstructures can be clearly identified.

These microscale thermophysical phenomena of bubble formation are summarized:

1. Individual, spherical vapor bubbles with diameters from 2 to 500 μm can be generated by solid-state polysilicon microheaters.
2. These thermal microbubbles may have controllable sizes by maintaining a small input power of tens of miliwatt.
3. The influence of Marangoni effect is strong within the temperature field generated by the microheaters.
4. Hysteresis phenomena of bubble nucleation have been observed.

Bubble Nucleation Mechanism

In order to investigate bubble nucleation mechanisms, both analytical and experimental approaches are conducted. For macroscale pool boiling experiments, heterogeneous nucleation theories have been based on saturated liquids [30−32].
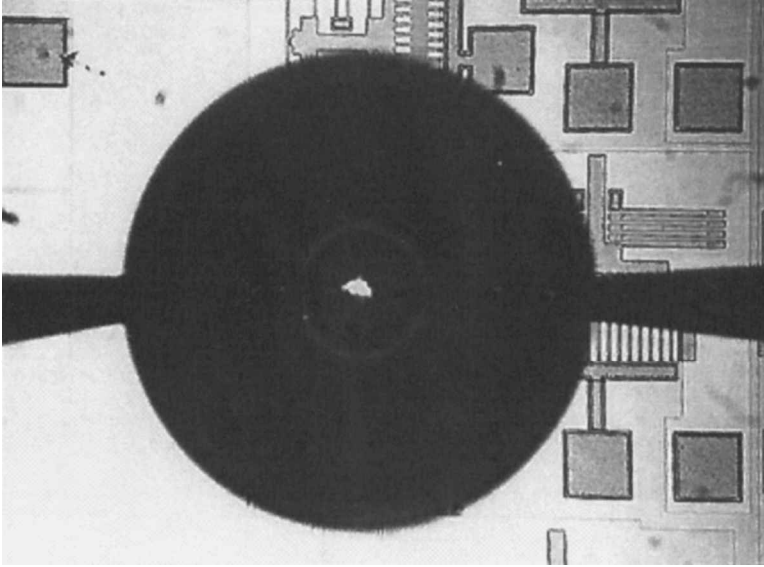
Figure 5. The final stage of a bubble before detaching.

Hsu's theory, which predicts the active cavity size for heterogeneous nucleation, has been analyzed here [31]. It should be noted that Hsu's theory and most other existing bubble nucleation theories are based on saturated pool boiling. These microheaters do not create the pool boiling condition during the experiments, however. Therefore, Hsu's theory may only provide the limiting case for predicting microscale bubble formation mechanism. The result of Hsu's analysis is shown in Figure 6, which used FC43 as the working liquid in simulation [16]. Both $r_{c,\mathrm{max}}$ and $r_{c,\mathrm{min}}$ are curves representing the critical, active cavity radii. It is observed that a superheat of about 20°C is necessary to activate cavities of 0.5 μm in radius. By examining fabricated microheaters as shown in Figure 3, cavities with 0.5 μm in radius are not likely to exist on these microheaters, which may have widths of only
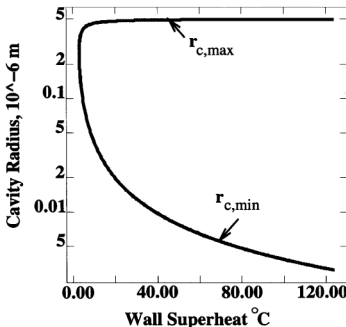

Figure 6. Effective sizes of cavities according to Hsu's theory in saturated FC 43 liquid.
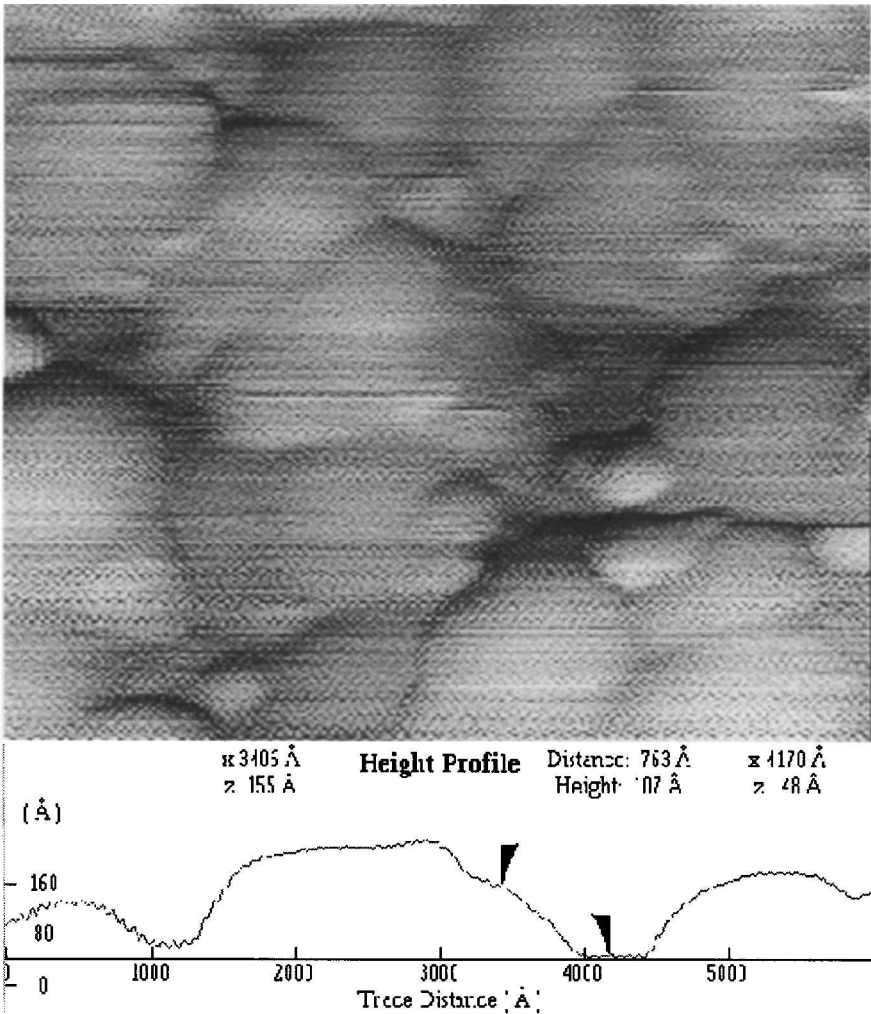
Figure 7. The AFM scanning result for the polysilicon microheater.

2 μm. An atomic force microscope (AFM) has been used in order to further characterize the surface of the microheaters. Figure 7 shows the AFM scanning result for an area of $0.6 \times 0.5 \ \mu m^2$. The root mean square (RMS) roughness is measured to be 6.5 nm. The lower graph of Figure 7 is a single scan over the center of the scanned area. A "cavity" shape may be identified, with peak-to-valley roughness of about 10.7 nm. If this cavity is activated during the bubble formation process, a superheat temperature of about 80°C should be reached, according to Hsu's analysis.

To further characterize the thermophysical bubble formation mechanism, temperature measurement is required. Due to the scale of microheaters, it is very difficult to measure the temperature precisely by introducing an external thermal

couple. The microresistor itself has been utilized as a thermistor, based on the experimental characterization of polysilicon resistivity constant with respect to temperature [33]. The onset bubble formation currents are measured for micro-heaters with different geometries, and corresponding temperatures are extracted by using the established electro-thermal model. It is found that bubble formation temperatures are close to the superheat limits for all tested liquids and are much higher than the predicted temperature suggested by Hsu's theory. Therefore, it is concluded that the microbubble formation mechanism using these microheaters is more likely quasi-homogeneous [34] nucleation than heterogeneous nucleation.

POTENTIAL AND FUTURE APPLICATIONS

The most successful application for thermal bubbles is the ink-jet printer. Tiny droplets are ejected by the power of thermal bubbles at a very high frequency for printing [5]. Recently, new technologies have led to advances in the manufacturing of ink-jet printer heads. For example, fabrication processes have been improved since the early ink-jet printers were introduced [35−38]. Different methods have been suggested to increase the density of ink droplets [39, 40], along with theoretical and experimental studies [41, 42]. The success of ink-jet printers has led to a promising future for other microfluidic machines based on thermal bubble formation. This section summarizes some potential and future applications.

In addition to the ejection of liquid droplets, phase-change phenomena have been applied to actuate micromechanical structures. In the late 1980s, Zdeblick and Angell demonstrated electric-to-fluidic membrane-type valves by using the thermal expansion and phase change of working liquids [43]. Their microvalves have been operated for a pressure up to 160 psi with turn-down ratio greater than 20,000:1. Lin and Pisano [13] have demonstrated bubble-powered microactuators by using the pressure of microbubbles to mechanically push microcantilever plates as illustrated in Figure 1b. The geometry of the actuator plate is $70 \times 60 \times 2$ μm^3, and it is suspended 2 μm above the substrate by connecting cantilever beams. A polysilicon microheater is fabricated on top of the substrate and beneath the actuator plate to generate thermal bubbles. Figure 8 shows the experimental result of a bubble-powered microactuator in which a thermal bubble underneath the plate is lifting the actuator plate vertically. A maximum vertical deflection of 140 μm and a force of 2 μN have been achieved.

Many different types of applications are currently under investigations. For example, microbubbles have also been used to move microstructures laterally in a micro steam engine [11]. In other applications, microbubbles have been proposed to expel liquid as pumping sources or mechanical valves in micromachined flow channels. There are different ways to construct microchannels [44, 45]. Figure 9 shows a cross-sectional view of a microchannel that was fabricated by a surface micromachining process [46]. The material of the microchannel is silicon nitride with a thickness of 1.7 μm on the cover and a width of 30 μm, height 6 μm (edge) to 7.5 μm (center). Preliminary experiments have demonstrated that microbubbles could have a preferred moving direction inside the microchannel, as seen in Figure 10. A bullet-shaped microbubble is formed inside the diverging-shape portion. This experiments have demonstrated that the walls of microflow channels constrain the
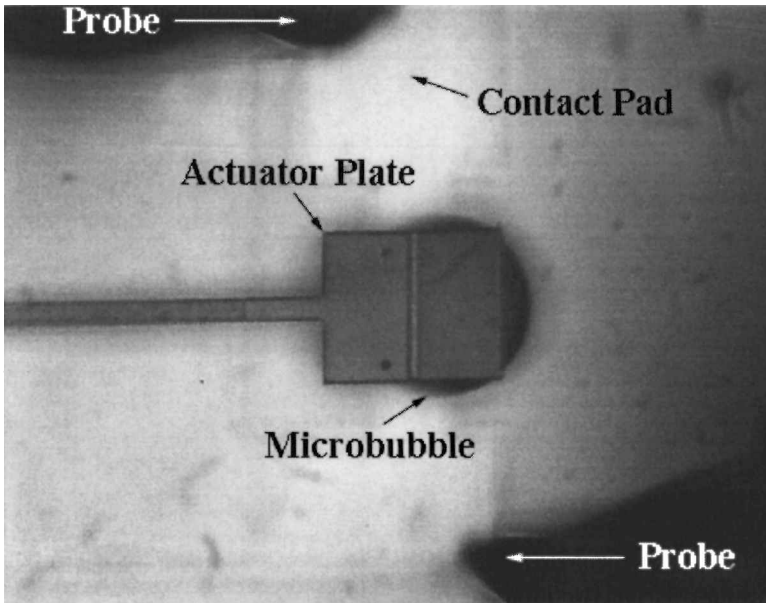
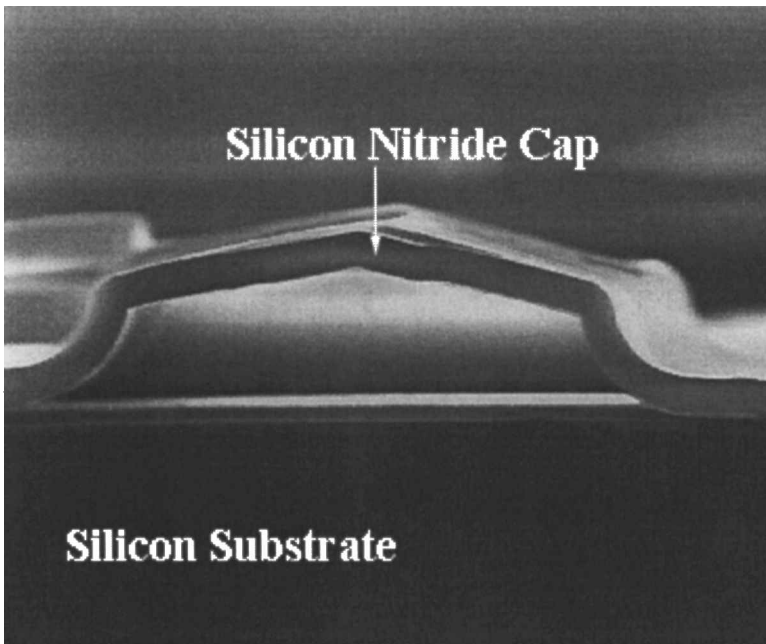**Figure 8.** A microbubble is lifting the actuator plate [13].

Figure 9. A cross-sectional SEM microphoto showing the microchannel [14].
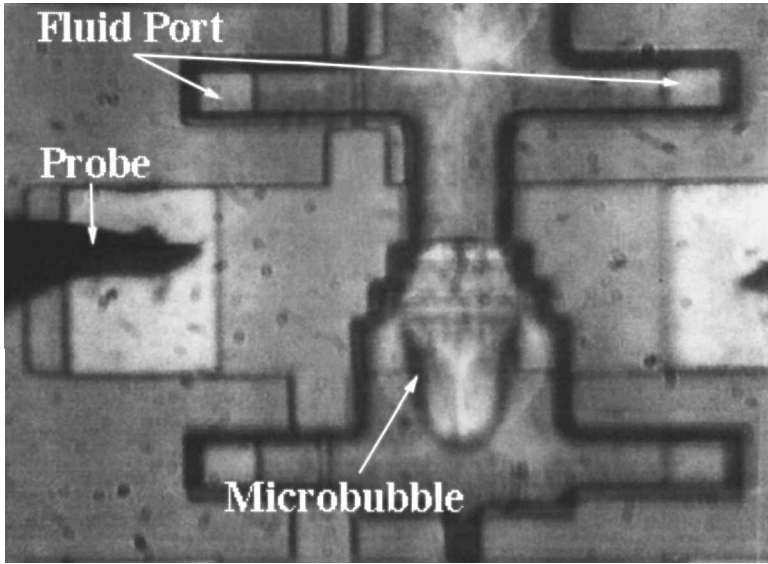
Figure 10. Microbubble with a bullet-like shape inside a microflow channel [14].

growth and movement of microbubbles. Therefore, these microbubbles are poten-
tially suitable as mechanical valves in microfluidic machines [14, 47].

   Microbubble pumping, on the other hand, has been proposed in the form of a
series of polycrystalline silicon strips running across the microchannels [10, 16].
These microheaters will generate microbubbles in sequence for pumping, and the
idea has been demonstrated preliminarily with both traversing microbubbles [48]
and diaphragms pumping [49] in microchannels. In addition to the above applica-
tions, bubble actuation forces have been applied in fluid mixers for chemical
analysis [47] and in fuel mixers inside the combustion chamber [50].

CONCLUSION

   The combination of microscale thermophysical phenomena and MEMS tech-
nologies provides unique opportunities for theoretical, experimental, and engineer-
ing challenges. This work addresses the thermophysical phenomena of bubble
formation by using solid-state microheaters and recommends specific directions for
future applications.

   Experimentally, individual, spherical vapor bubbles with diameters of 2 to 500
μm have been generated, and unusual characteristics such as stable and control-
lable bubbles have been demonstrated. The theoretical bases of microscale heat
transfer are introduced by a one-dimensional heat equation, which is also used for
measuring the onset bubble formation temperatures. Bubble nucleation mecha-
nisms by microheaters are discussed with models developed for macroscale boiling
experiments, and it is concluded that homogeneous nucleation is the likely mecha-
nism for bubbles generated by microheaters. Challenging applications based on

microbubble formation are illustrated, including microbubble-powered actuators, microbubble valves, and microbubble pumps.

Before bubble-powered micromachines can be optimally designed and operated, microscale thermophysical phenomena should be carefully investigated in both theoretical and experimental regimes. Specific areas to be explored are:

- Schemes for temperature measurements down to 1 μm for locations on microheaters and the surrounding environment
- Models for bubble incipience mechanisms by using microheaters and under subcooled boiling conditions
- Transport processes of vaporization and condensation before and after bubble formation
- Microfluid flows and thermocapillary forces generated by the local temperature field including the existence of microbubbles
- Fluid flows induced by microbubble formation both with and without the constraint of microchannels

REFERENCES

1. K. E. Peterson, Silicon as a Mechanical Material, *Proc. IEEE*, vol. 70, pp. 420–457, 1982.
2. Y. Bayazitoglu and G. P. Peterson (eds.), Fundamental Issues in Small Scale Heat Transfer, *ASME Winter Annual Meeting*, HTD-227, 1992.
3. F. M. Gerner and K. S. Udell (eds.), Heat Transfer on the Microscale, *29th Natl. Heat Transfer Conf.*, HTD-253, 1993.
4. C. L. Tien, Recent Developments in Microscale Heat Transfer, *Proc. 1996 4th Int. Symp. on Heat Transfer*, pp. 1–16, 1996.
5. N. J. Nielsen. History of Thinkjet Printerhead Development, *HP Journal*, vol. 36, no. 5, pp. 4–10, 1985.
6. R. R. Allen, J. D. Meyer, and W. R. Knight, Thermodynamics and Hydrodynamics of Thermal Ink Jets, *HP Journal*, vol. 36, no. 5, pp. 21–27, 1985.
7. L. Lin and A. P. Pisano, Bubble Forming on a Micro Line Heater, *Proc. ASME Winter Annual Meeting, Micromechanical Sensors, Actuators and Systems*, DSC-32, pp. 147–163, 1991.
8. R. C. Jaeger. *Introduction to Micro Electronic Fabrication*, Addison-Wesley, Reading, MA, 1988.
9. L. Lin, A. P. Pisano, and A. P. Lee, Microbubble Powered Actuator, *Digest of Transducers '91, Int. Conf. on Solid-State Sensors and Actuators*, pp. 1041–1044, 1991.
10. L. Lin, A. P. Pisano, and R. S. Muller, Silicon Processed Microneedles, *Digest of Transducers '93, Int. Conf. on Solid-State Sensors and Actuators*, pp. 237–240, 1993.
11. J. J. Sniegowski, A Micro Actuation Mechanism Based on Liquid-Vapor Surface Tension, *Digest of Late News of Transducers '93, Int. Conf. on Solid-State Sensors and Actuators*, pp. 12–13, 1993.
12. S. M. Sze, *VLSI Technology*, 2d ed., McGraw-Hill, New York, 1988.
13. L. Lin and A. P. Pisano, Thermal Bubble Powered Microactuators, *Microsystem Technol.*, vol. 1, pp. 51–58, 1994.
14. L. Lin, K. S. Udell, and A. P. Pisano, Liquid-Vapor Phase Transition and Bubble Formation in Micro Structures, *Thermal Sci. Eng.*, vol. 2, pp. 52–59, 1994.
15. W. Riethmuller and W. Benecke, Thermally Excited Silicon Microactuators, *IEEE Trans. Electron Devices*, ED-35, pp. 758–762, 1988.

16. L. Lin, *Selective Encapsulations of MEMS: Micro Channels, Needles, Resonators and Electromechanical Filters*, Ph.D. thesis, University of California, Berkeley, 1993.

17. J. P. Holman, *Heat Transfer*, 7th ed., McGraw-Hill, New York, 1990.

18. S.-S. Seung, S.-D. Oh, and H.-Y. Kwak, A Model of Bubble Nucleation on a Micro Line Heater, *Proc. ASME Winter Annual Meeting, Micromechanical Sensors, Actuators and Systems*, DSC-40, pp. 313−328, 1992.

19. S.-K. Cho, S.-D. Oh, S.-S. Seung, and H.-Y. Kwak, Actuation Mechanism by Bubble Formation on a Micro Line Heater, *Proc. ASME Winter Annual Meeting, Micromechanical Sensors, Actuators and Systems*, DSC-46, pp. 35−62, 1992.

20. C. C. Pitts and G. Lepert, The Critical Heat Flux for Electrically Heated Wires in Saturated Pool Boiling, *Int. J. Heat Mass Transfer*, vol. 9, pp. 365−377, 1966.

21. K. H. Sun and J. H. Lienhard, The Peak Pool Boiling Heat Flux on Horizontal Cylinders, *Int. J. Heat Mass Transfer*, vol. 13, pp. 1425−1439, 1970.

22. N. Bakhru and J. H. Lienhard, Boiling from Small Cylinders, *Int. J. Heat Mass Transfer*, vol. 15, pp. 2011−2025, 1972.

23. E. Baker, Liquid Cooling of Microelectronic Devices by Free and Forced Convection, *Microelectronics and Reliability*, vol. 11, pp. 213−222, 1972.

24. C.-F. Ma and A. E. Bergles, Jet Impingement Nucleate Boiling, *Int. J. Heat Mass Transfer*, vol. 29, pp. 1095−1011, 1986.

25. T. K. Lee, T. W. Simon, and A. Bar-Cohen, An Investigation of Short Heating Length Effect on Flow Boiling Critical Heat Flux in a Subcooled Turbulent Flow, in *Cooling Technology for Electronic Equipment*, W. Aung (ed.), pp. 435−450, Hemisphere, Washington, DC, 1988.

26. H. B. Clark, P. S. Strenge, and J. W. Westwater, Active Sites for Nucleate Boiling, *Chem. Eng. Prog. Symp.*, vol. 55, pp. 103−110, 1959.

27. S. Stralen and R. Cole, *Boiling Phenomena: Physicochemical and Engineering Fundamentals and Applications*, Hemisphere, Washington, DC, 1979.

28. V. P. Carey, *Liquid-Vapor Phase-Change Phenomena*, Hemisphere, Washington, DC, 1992.

29. 3M Company, *Fluorinert Electronic Liquids Product Manual*, 3M Industrial Chemical Production Division, St. Paul, MN, 1991.

30. Zuber, Vapor Bubbles in Non-uniform Temperature Field, *Int. J. Heat Mass Transfer*, vol. 2, p. 83, 1961.

31. Y. Y. Hsu, On the Size Range of Active Nucleation Cavities on a Heating Surface, *J. Heat Transfer*, vol. 84C, pp. 207−216, 1962.

32. B. B. Mikic, W. M. Rohsenow, and P. Griffith, On Bubble Growth Rate, *Int. J. Heat Mass Transfer*, vol. 13, pp. 657−666, 1970.

33. L. Lin and M. Chiao, Electrothermal Responses of Lineshape Microstructures, *Sensors and Actuators*, vol. A55, pp. 35−41, 1996.

34. H. Merte, Jr., and H. S. Lee, Quasi-homogeneous Nucleation in Microgravity at Low Heat Flux: Experiments and Theory, *J. Heat Transfer*, vol. 119, pp. 305−312, 1997.

35. R. Askeland, W. Childers, and W. Sperry, The Second Generation Thermal Inkjet Structure, *HP Journal*, pp. 376−384, August 1988.

36. J. S. Aden, J. H. Bohorquez, D. M. Crook, A. Gacia, and U. E. Hess, The Third Generation Thermal Inkjet Structure, *HP Journal*, pp. 41−45, February 1994.

37. C. C. Beatty, A Chronology of Thermal Ink-Jet Structures, *Technical Digest of IEEE Solid-State Sensor and Actuator Workshop*, pp. 200−204, June 1996.

38. D. Westberg and G. I. Andersson, A Novel CMOS-Compatible Inkjet Head, *Digest of Transducers '97, Int. Conf. on Solid-State Sensors and Actuators*, pp. 813−816, 1997.

39. J. Chen and K. Wise, A High-Resolution Silicon Monolithic Nozzle Array for Inkjet Printing, *Digest of Transducers '95, Int. Conf. on Solid-State Sensors and Actuators*, pp. 321−324, 1995.

40. J. D. Lee, H. D. Lee, H. J. Lee, J. B. Yoon, K. H. Han, J. K. Kim, C. K. Kim, and C. H. Han, A Monolithic Thermal Inkjet Printhead Utilizing Electrochemical Etching and Two-Step Electroplating Techniques, *Proc. 1995 Int. Electron Devices Meeting*, vol. 1024, pp. 601−604, 1995.

41. A. Asai, Bubble Dynamics in Boiling under High Heat Flux Pulse Heating, *J. Heat Transfer*, vol. 113, pp. 973−979, 1991.

42. M. O'Horo and J. Andrews, Initial Stages of Vapor-Bubble Nucleation in Thermal Ink-Jet Processes, *Proc. SPIE*, vol. 2413, pp. 182−188, 1995.

43. M. J. Zdeblick and J. B. Angell, A Microminiature Electric-to-Fluidic Valve, *Digest of Transducers '87, Int. Conf. on Solid-State Sensors and Actuators*, pp. 827−829, 1987.

44. T. L. Hoopman, Microchanneled Structures, *Proc. ASME Winter Annual Meeting, Micromechanical Sensors, Actuators and Systems*, DSC-19, pp. 171−174, 1990.

45. J. Pfahler, H. Bau, J. Harley, and J. Zemel, Liquid Transport in Micron and Submicron Channels, *Sensors and Actuators A—Physical*, vol. 22, pp. 431−434, 1990.

46. L. Lin, K. S. Udell, and A. P. Pisano, Vapor Bubble Formation on a Micro Heater in Confined and Unconfined Micro Channels, *Proc. ASME 29th Natl. Heat Transfer Conf.*, HTD-Vol. 253, pp. 85−94, 1993.

47. J. Evans, D. Liepmann, and A. P. Pisano, Planar Laminar Mixer, *Proc. IEEE Micro Electro Mechanical Systems (MEMS97)*, pp. 96−101, 1997.

48. T. K. Jun and C.-J. Kim, Microscale Pumping with Traversing Bubbles in Microchannels, *Solid-State Sensors and Actuators Workshop*, pp. 144−147, 1996.

49. H. Mizoguchi, M. Ando, T. Mizno, T. Takagi, and N. Nakajima, Design and Fabrication of Light Driven Micropump, *Proc. IEEE Micro Electro Mechanical Systems (MEMS92)*, pp. 31−36, 1992.

50. F.-G Tseng, C. Linder, C.-J. Kim, and C.-M. Ho, Control of Mixing with Micro Injectors for Combustion Application, *ASME Int. Mechanical Engineering Congress and Exposition*, DSC-Vol. 59, pp. 183−187, 1996.